University of Baghdad
College of Engineering
JOURNAL OF ENGINEERING

Journal of Engineering

journal homepage: www.joe.uobaghdad.edu.iq

Volume 28 Number 10 October 2022

Civil and Architectural Engineering

Parameters Affecting the Strength and Behavior of RC Dapped-End Beams: A Numerical Study

Arten N. Atalla *	**Khalaf I. Mohammad**
B Sc in Civil Engineering	Ph.D. in Civil Engineering
University of Mosul	University of Mosul
College of Engineering	College of Engineering
Department of Civil Engineering	Department of Civil Engineering
Mosul, Iraq	Mosul, Iraq
artn.20enp113@student.uomosul.edu.iq	kimjebouri@uomosul.edu.iq

ABSTRACT

The finite element method has been used in this paper to investigate the behavior of precast reinforced concrete dapped-ends beams (DEBs) numerically. A parametric investigation was performed on an experimental specimen tested by a previous researcher to show the effect of numerous parameters on the strength and behavior of RC dapped-end beams. Reinforcement details and steel arrangement, the influence of concrete compressive strength, the effect of inclined load, and the effect of support settlement on the strength of dapped-ends beams are examples of such parameters. The results revealed that the dapped-end reinforcement arrangement greatly affects the behavior of dapped end beam. The failure load decreases by 25% when insufficient development length for main dapped-end reinforcement is provided, and nib shear reinforcement has less effect than nib main reinforcement. The results also showed that the shear strength of dapped-end beams increased as concrete strength increased. When the compressive strength of concrete increased by 100% led to an enhancement of strength capacity by about 34%. The strength of the dapped-ends beams is significantly affected by the settlement of the supports.

Keywords: Finite Element, Dapped-ends beams, concrete compressive strength, support settlement.

المتغيرات المؤثرة على مقاومة وسلوك العتبات الخرسانية المسلحة ذات النهايات المقضومة– دراسة عددية

*Corresponding author
Peer review under the responsibility of University of Baghdad.
https://doi.org/10.31026/j.eng.2022.10.06

Article received: 23/4/2022
Article accepted: 26/7/2022
Article published: 1/10/2022

*** ارتن نجيب عطاالله** بكالوريوس هندسة مدنية جامعة الموصل كلية الهندسة قسم الهندسة المدنية	**خلف إبراهيم محمد** دكتوراه هندسة مدنية جامعة الموصل كلية الهندسة قسم الهندسة المدنية

الخلاصة

تم استخدام طريقة العناصر المحددة في هذا البحث للتحقق عدديا من السلوك العددي للأعتاب الخرسانية المسلحة مسبقة الصب ذوات النهايات المقضومة. سيتم إجراء دراسة بارا مترية على عينة تجريبية تم اختبارها بواسطة باحث سابق لإظهار تأثير العديد من المتغيرات على مقاومة وسلوك الأعتاب الخرسانية المسلحة ذوات النهايات المقضومة. تفاصيل وترتيب حديد التسليح، وتأثير مقاومة انضغاط الخرسانة، وتأثير الحمل المائل وتأثير هبوط المساند على مقاومة وسلوك الأعتاب الخرسانية المسلحة ذوات النهايات المقضومة هي أمثلة على هذه المتغيرات. اظهرت النتائج أن ترتيب حديد التسليح له تأثير كبير على سلوك العتبات الخرسانية المسلحة ذوات النهايات المقضومة .انخفض حمل الفشل بنسبة 25% عند عدم وجود طول تثبيت كاف للتسليح الرئيسي للنهاية المقضومة تأثير اقل من تسليحها الرئيسي. كما أظهرت النتائج أيضًا أن مقاومة القص للأعتاب الخرسانية المسلحة ذوات النهايات المقضومة تزداد كلما تزداد مقاومة انضغاط الخرسانة، فعند زيادة مقاومة الانضغاط الخرسانية بنسبة 100% أدت الى زيادة مقاومة العتبة بنحو34%. وتتأثر مقاومة وسلوك الأعتاب الخرسانية المسلحة ذوات النهايات المقضومة بشكل كبير عند وجود هبوط في المساند.

الكلمات المفتاحية: العناصر المحددة، العتبات ذوات النهايات المقضومة، مقاومة انضغاط الخرسانة، هبوط المساند.

1. INTRODUCTION

Reinforced concrete dapped-end beams (RC-DEBs) are widely used in the reinforced concrete construction of bridge girders in the form of precast. Girders with dapped ends are normally used in parking structures, pedestrian bridges, and long-span bridges. Dapped ends also serve as popular details for building and bridges' expansion joints. Using RC-DEBs provides advantages such as better lateral stability of structural elements at the supports and reducing floor to floor height which leads to cutting the total height of the structure and consequently decreasing the total dead load. **(Aswin, et al., 2015)**

Examples of dapped-end applications are:

1- As a cantilever and suspended span type of structure (**Fig. 1**).
2- As a drop-in beam between corbels (**Fig. 2**).
3- As a hide-away type of beam-to-beam and beam-to-column connection (**Fig. 3**).

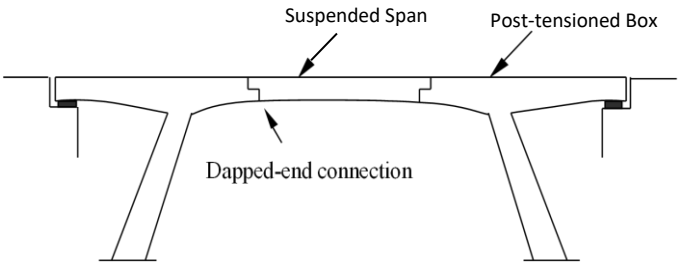

Figure 1. As a cantilever suspended span bridge. **(Huang and Nanni, 2015)**

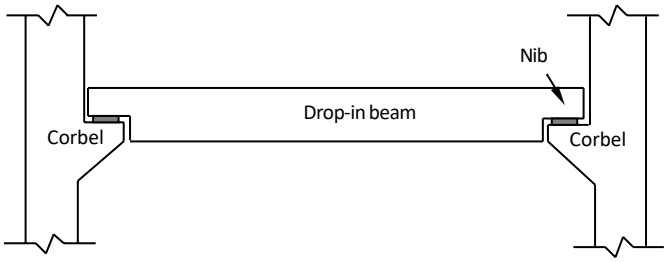

Figure 2. As a drop-in beam supported by corbels. **(Huang and Nanni, 2015)**

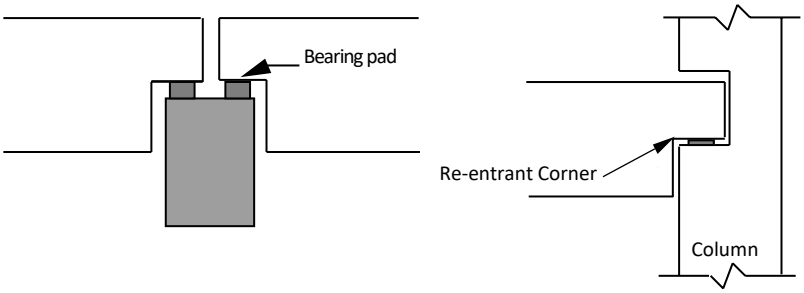

Figure 3. As a hide -away type connection. **(Huang and Nanni, 2015)**

Historically, dapped-end beams have been investigated with various detailing and analytical approaches. **(Lu et al., 2003)** tested dapped-ends beams to study their shear strength capacity, and they concluded that the shear strength of dapped-end beams increases with increasing concrete compressive strength and nib flexural reinforcement area and increases with decreasing nominal shear span-depth ratio. Meantime, **(Wang and Hoogenboom 2005)** have reported that the shear strength capacity of RC dapped-ends beams is increased by enhancement of the nib height, nominal shear span, or amount of hanger reinforcements. By using diagonal reinforcement through the reentrant corners, shear strength capacity can be increased. **(Taher, 2005)** investigated the different strengthening techniques of RC-DEBs to enhance the shear strength capacity. It has been reported that all the strengthening methods are enhancing the shear strength capacity of RC-DEBs. **(Peng, 2009)** performed experimental tests to study the effect of detailing on the behavior of dapped-end beams. The results showed that the details and anchorage of longitudinal and hanger reinforcement have an important effect on the ductility and shear strength of the dapped-end beams. **(AlSabawy, 2011)** Studied the nonlinear three-dimensional finite element analysis of reinforced concrete dapped end beam. The predicted loads of the reinforced concrete dapped-end beams by the present finite element models at various stages were found to be in good agreement with the previous test data. The failure mechanism of reinforced concrete dapped-end beams is modeled quite well using the present finite element model. The failure load predicted is very close to the failure load of previous experimental studies. The shear strength of the dapped-end beams linearly increases with the increase of the concrete strength. **(Nagrodzka and Piotrokowski, 2012)** investigated experimentally the reinforced concrete (RC) dapped-end beams loaded with inclined forces compared to identical ones loaded with vertical forces only. They concluded that in the dapped-end beam loaded with inclined force, the crack patterns differed from those observed in dapped ends loaded with vertical forces. Imposing an additional horizontal force equal to one-half of the component vertical force caused a 25% decrease in the load capacity. **(Lu et al., 2015)** tested 24 reinforced concrete dapped-end beams. The main variables studied were the concrete compressive strength, the shear span-to-depth ratio and the horizontal loads. The test results

indicate that the shear strength of dapped-end beams increases with an increase in concrete compressive strength and increases with decreases in shear span-to-depth ratio and horizontal load. **(Shakir et al., 2020)** studied the effect of opening characteristics on the performance of high-strength dapped-end beams. They concluded that the location and size of rectangular openings in the deep portion of the dapped-end beam greatly influence the shear strength and failure load. **(Sabre et al., 2021)** studied the effect of support settlement and their types on the failure load of dual span continuous deep beam using nonlinear finite element ANSYS program. It was observed that there was a marked variation in the value of the failure load under the influence of different support conditions and the support settlement that occurs in them.

2. DESCRIPTION OF THE ANALYZED BEAM

Experimental test specimens investigated by (**Taher, 2005)** are adopted in this study. Three main defects were intentionally introduced at the recess zone, including an inadequate development length of bottom longitudinal reinforcement at the dapped ends and elimination of either horizontal or vertical shear reinforcement at the ends. The dapped ends were divided into four groups, as shown in **Fig. 4**, with respect to the defect inherited due to reinforcement detailed as follows:

1- Group I: (Control sample) conventionally detailed reinforcement with adequate development length of the longitudinal tension reinforcement beyond the reentrant section with both vertical stirrups and horizontal side reinforcement provided at the dapped zone.
2- Group II: similar to Group I, but with insufficient development length of the longitudinal tension reinforcement beyond the reentrant section.
3- Group III: similar to Group I, but without horizontal side reinforcement in the recess zone.
4- Group IV: similar to Group I, but without vertical stirrups in the recess zone.

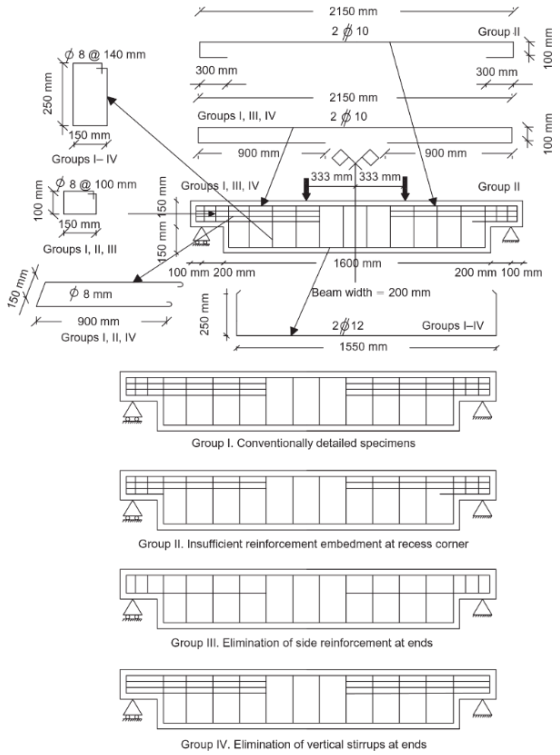

Figure 4. Reinforcement details of the four experimental groups **(Taher, 2005).**

3. FINITE ELEMENT MODELING

Defining elements includes dividing the shape into small parts (finite elements), and each of these elements consists of a set of nodes through which the elements are connected together to give the desired structure shape. The finite element method is one of the numerical analysis methods adopted in analyzing many engineering problems, including the nonlinear numerical analysis of reinforced concrete dapped-ends beams. And among these programs, ANSYS is one of the most important and widespread programs in the analysis of reinforced concrete members, which depends on the method of finite elements in the analysis of the structure **(Al – Sherrawi and Shanshal, 216)**.

3.1 Element Types

To model the precast reinforced concrete dapped-end beam in the finite element method using the ANSYS software, the necessary elements must be selected to ensure conformity between the model and reality. ANSYS provides an element known as a SOLID 65 to model concrete. This element has eight nodes with three degrees of freedom at each node (translations in the nodal x, y, and z directions). Plastic deformation, cracking in three orthogonal directions, and crushing are the most important capability of this element which make it a suitable choice to model concrete material. The 3D spar element (LINK 180) was used for steel reinforcement, which allows the elastic-perfectly plastic response of the reinforcing bars. This element is a uniaxial tension-compression element, and two nodes are required for this element; each node has three degrees of freedom translations in the nodal x, y, and z directions **(Mohammed and Mahmoud, 2015)**. The Spring element (COMBINED14) is used to model the elastic support. This element is a one-dimensional linear element that has the ability of elongation and rotation. This element consists of two nodes at both ends. Each node has three DOF, displacement (u, v, w) in x, y, and z directions, respectively, and cannot bend or torsion and has the ability of rotation. Typical modeling of the beam and elastic support is shown in **Fig.5.**

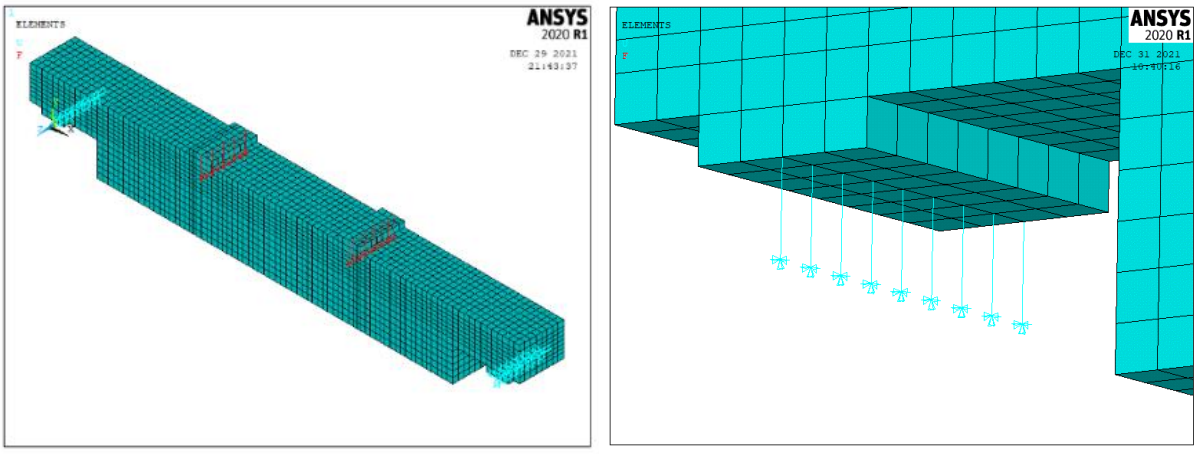

(a) (b)

Figure 5. a) Typical modeling for the control sample. b) Modeling of elastic support (Spring).

3.2 Material Properties

3.2.1 Concrete

In ANSYS, Concrete needs two properties to be modeled properly, linear isotropic and nonlinear. Linear properties are elastic modulus (E_c) and Poisson's ratio (ν). Poisson's ratio for concrete under uniaxial compression loading ranges between 0.15 to 0.22, a representative value is 0.2 **(Chen, 1982)**. The initial modulus of elasticity of concrete (E_c) is highly dependent on its compressive strength, and it can calculate with acceptable accuracy from the empirical formula **(ACI Committee, 2019)**:

$$E_c = 0.043 * w_c^{1.5} * \sqrt{fc'} \quad (1)$$

And when normal weight aggregate is used in concrete, the formula becomes:

$$E_c = 4700 * \sqrt{fc'} \quad (2)$$

where:
E_c is the initial modulus of elasticity of concrete in MPa.
w_c is the unit weight of concrete in Kg/m^3
fc' is uniaxial compressive cylinder strength of concrete in MPa.

The multi-linear isotropic properties use the Von Mises failure criterion along with the **(William and Warnke, 1975)** model to define the failure of the concrete. ANSYS requires the uniaxial stress-strain relationship of normal concrete in compression. Numerical expressions **(Desayi, 1964)**. Eq. 3 and 4 were used along with Eq. 5 **(Gere and Timoshenko, 1997)** to construct the uniaxial compressive stress-strain curve of normal concrete in this study.

$$f = \frac{E_c \varepsilon}{1+\left(\frac{\varepsilon}{\varepsilon_o}\right)^2} \quad (3)$$

$$\varepsilon_o = \frac{2f_c'}{E_c} \quad (4)$$

$$E_c = \frac{0.3f_c'}{\varepsilon} \quad (5)$$

where:
f = stress at any strain ε, MPa
ε = strain at any stress f
ε_o = strain at the ultimate compressive strength (fc').

Uniaxial stress-strain curve of normal concrete fc' = 25 MPa is shown in **Fig.6.**
For high strength concrete (HSC), **(Fib-Bulletin 42, 2008)** code equations must be used to draw the stress-strain relationship **(Mahmood and Mohammad, 2019)**. The stress-strain relationship may be approximated by Eq. 6. The strain ε_{c1} at maximum compressive stress is increasing with increasing compressive strength. Values for ε_{c1} under short-term loading is given in **Table 1**

following the proposal from **(Propovic, 1973)** and **(Meyer, 1998)**. The uniaxial stress-strain diagram of HSC is shown in **Fig.7.**

$$\frac{\sigma_c}{f_c} = -\frac{k \cdot \eta - \eta^2}{1 + (k-2) \cdot \eta} \; for \; |\varepsilon_c| < |\varepsilon_{c,lim}| \quad (6)$$

Where: $\eta = \varepsilon_c / \varepsilon_{c1}$

$\varepsilon_{c1} = -1.60(f_{cm}/10\ \text{MPa})^{0.25}/1000$ strain at maximum compressive stress

$k = E_{ci}/E_{c1}$ Plasticity number

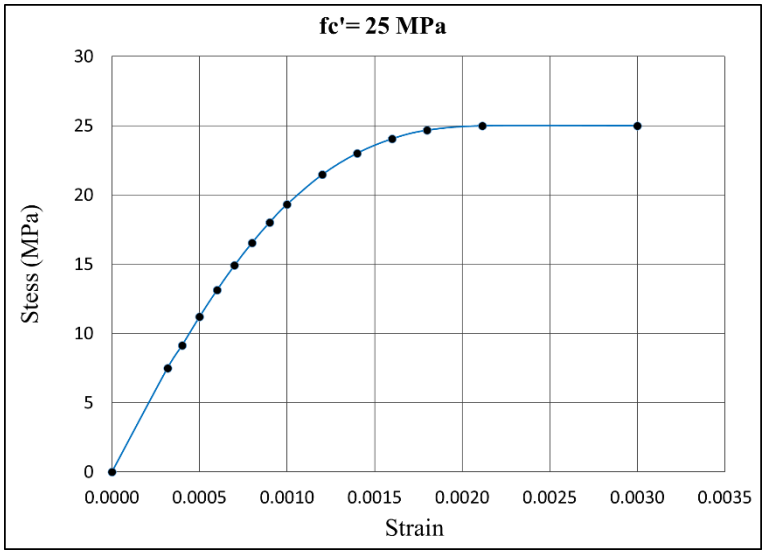

Figure 6. Uniaxial stress-strain relationship of normal concrete.

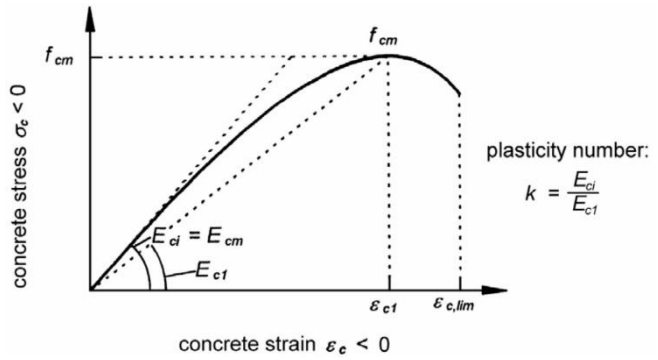

Figure 7. Uniaxial stress-strain relationship of high strength concrete. **(Fib-Bulletin 42, 2008)**

Table 1. Tangent modulus E_{ci}, E_{c1}, ε_{c1} and $\varepsilon_{c,lim}$ for the various concrete grades **(Fib-Bulletin 42, 2008)**

Concrete grade	C20	C30	C40	C50	C70	C90	C120
E_{ci} [GPa]	28.9	32.0	34.6	36.8	40.7	43.9	48.0
E_{c1} [GPa]	13.5	17.0	20.3	23.4	29.2	34.6	42.7
ε_{c1} [‰]	-2.07	-2.23	-2.37	-2.48	-2.67	-2.83	-3.0
$\varepsilon_{c.lim}$ [‰]	-3.5	-3.5	-3.5	-3.4	-3.2	-3.0	-3.0

$k = E_{ci}/E_{c1}$	2.14	1.88	1.71	1.58	1.39	1.27	1.12

3.2.2 Steel plates

The steel plates were added at the locations of supports and applied loads to avoid stress concentration in these locations and provide good stress distribution. The elastic modulus of a steel plate is 200,000 MPa, and its Poisson's ratio is 0.3, which was used in the ANSYS model.

3.2.3 Steel reinforcement

The steel reinforcement is assumed to be elastic-perfectly plastic material and identical in tension and compression. The modulus of elasticity of steel is equals to 200,000 MPa and its Poisson's ratio is equals to 0.3. The yield stress of each type was equals to 400 MPa for the main reinforcement and 280 MPa for stirrups reinforcement.

4. RESULTS COMPARISON AND DISCUSSION

4.1 Load-Deflection Response

Load-midspan deflection curves for each group were obtained from finite element analysis and compared with the experimental results shown in Fig. 8, **Fig. 9,** and **Table 2**.

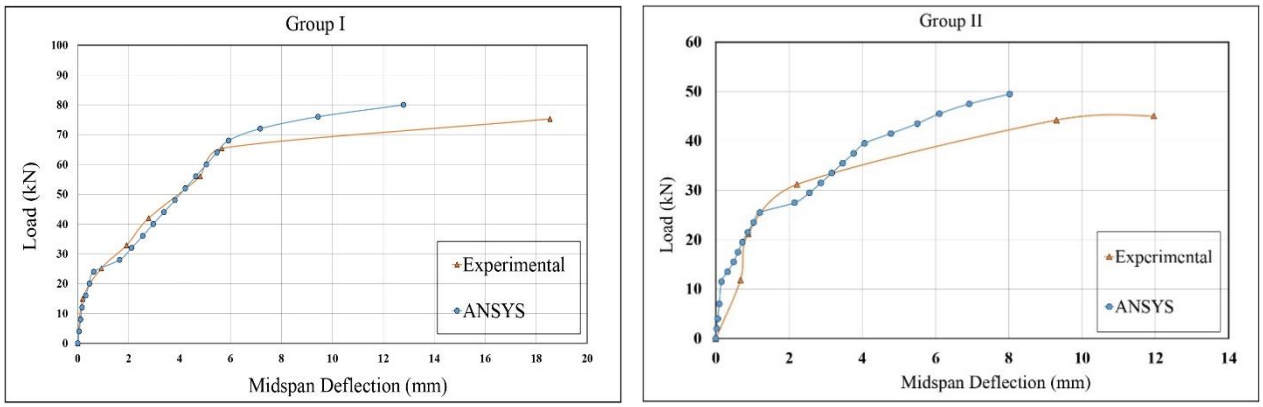

(a) (b)

Figure 8. Load-deflection curve for a) group I and b) group II

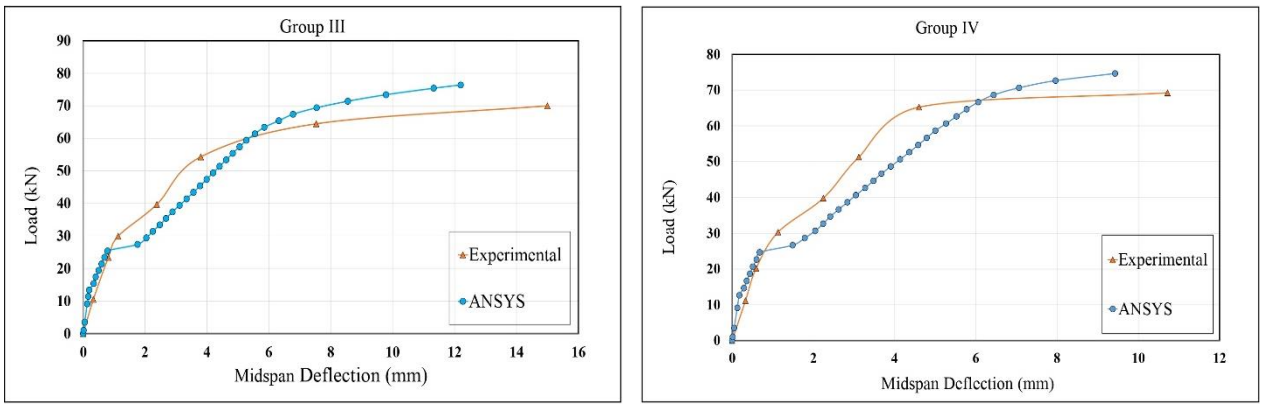

(a) (b)

Figure 9. Load-deflection curve for a) group III and b) group IV.

Table 2. Comparison between failure results of experimental and ANSYS

Group	Experimental Failure Load (kN)	ANSYS Load (kN)	ANSYS / Experimental	Experimental Failure Deflection (mm)	ANSYS Deflection (mm)	ANSYS / Experimental
I	75	80.00	1.06	18.5	12.789	0.69
II	45	49.5	1.10	16.75	8.024	0.48
III	70	76.403	1.09	15.01	12.198	0.81
IV	69	74.565	1.08	14.34	9.427	0.66

From **Fig. 8-a,** it can be seen that at a load of 72 kN, the beam is closing to failure because an evident increase in deflection accompanies the slight increase in loads; this occurs because of the flexural reinforcement (A_f) of group I is yielding, and the point of 72 kN is called the yielding point, while the yielding point of main reinforcement (A_s) at a load of 76 kN.
In group II, the flexural reinforcement (A_f) and the main reinforcement (A_s) did not reach yielding because of insufficient development length, while the hanger reinforcement (A_h) yielded.
The yielding points of group III in flexural and main reinforcement are 67 kN and 62.5kN, respectively. In the last group (IV), the yielding point in flexural reinforcement was at 69.5 kN, while the yielding point of main reinforcement was at 70 kN.
From **Table 2** and **Fig.8,** and **Fig. 9**, it seems to be good concurrence between experimental and ANSYS results, especially for the first group.
Group I give the max failure load and maximum midspan deflection because the sample has sufficient main reinforcement (A_s) embedment beyond the reentrant corner (suitable development length) and suitable nib reinforcement than any other group.
Group II has the minimum value of failure load because of insufficient main reinforcement embedment beyond the reentrant corner.
The decrease in failure load of group III, and IV than in group I because there is missing horizontal side reinforcement and vertical shear reinforcement in the recess zone of group III and IV, respectively, with the group I, which has both of these items in its reinforcement.
As a result, the load-deflection curve of group I is the most conformable curve between experimental results and ANSYS results than the four curves so we will depend on this group (group I) for the parametric study to predict the effect of various parameters on DEBs in the next step.

4.2 Stresses in Concrete and Steel

The stresses in concrete and steel are obtained from the FE analysis by ANSYS at the load step that precedes the last step (directly before failure). These stresses are shown in **Fig. 10** through **Fig. 13**.

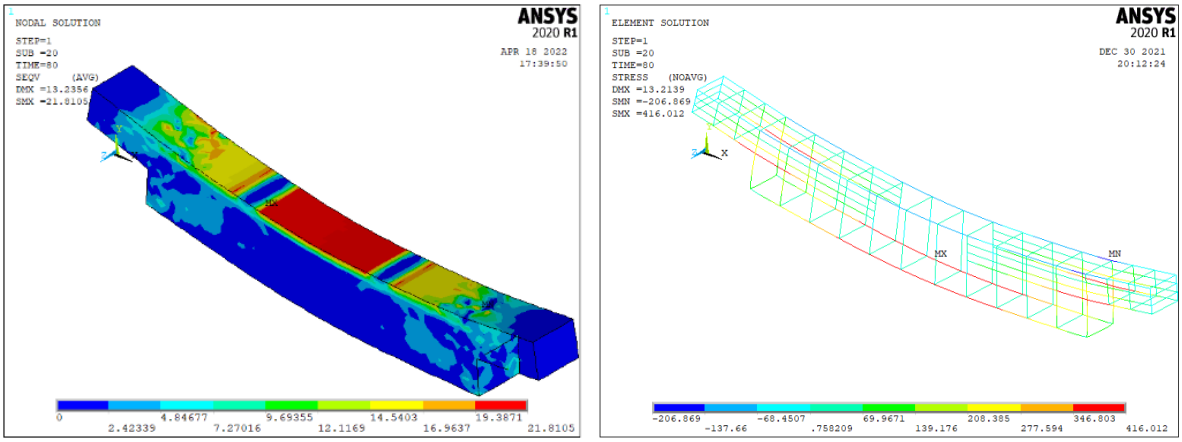

(a) (b)

Figure 10. Stresses in FE model group I. (a) Concrete Von Mises stresses, (b) Steel stresses.

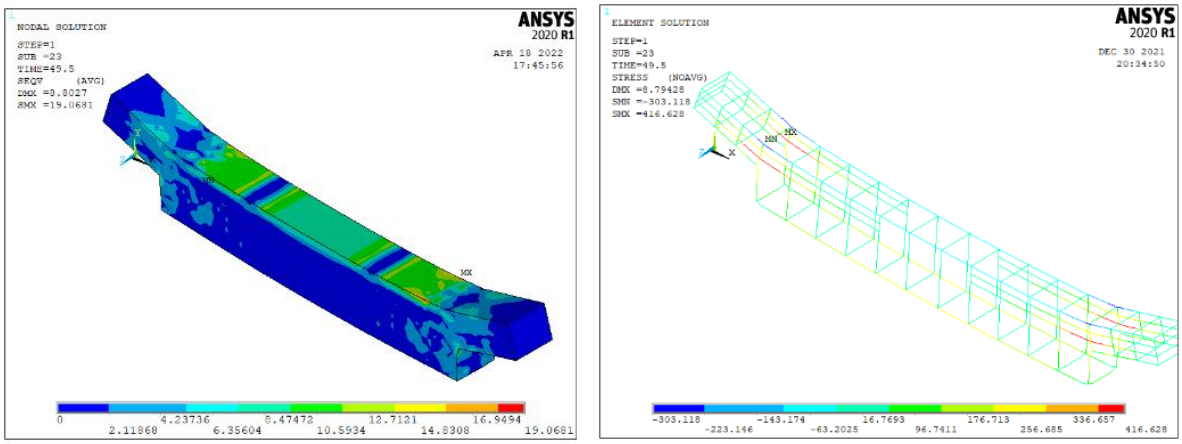

(a) (b)

Figure 11. Stresses in FE model group II. (a) Concrete Von Mises stresses, (b) Steel stresses

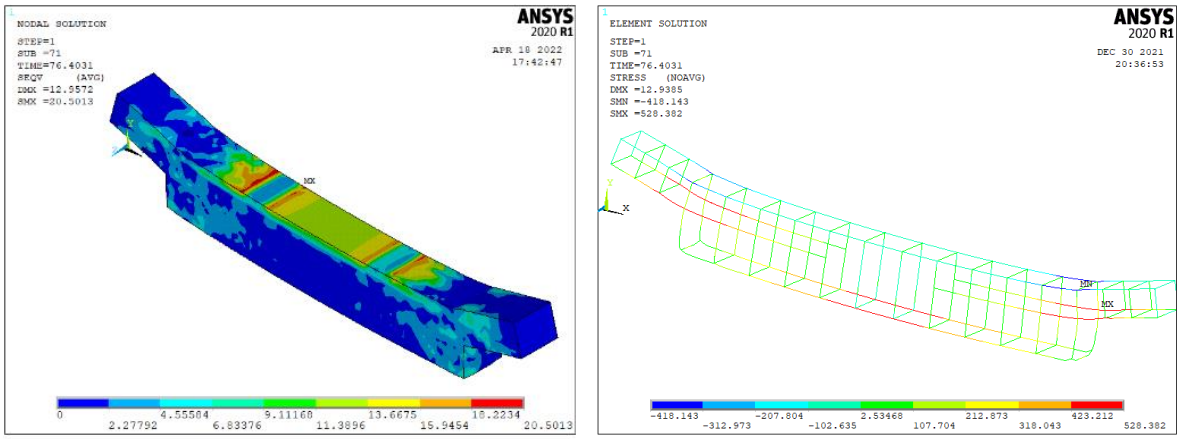

(a) (b)

Figure 12. Stresses in FE model group III. (a) Concrete Von Mises stresses, (b) Steel stresses

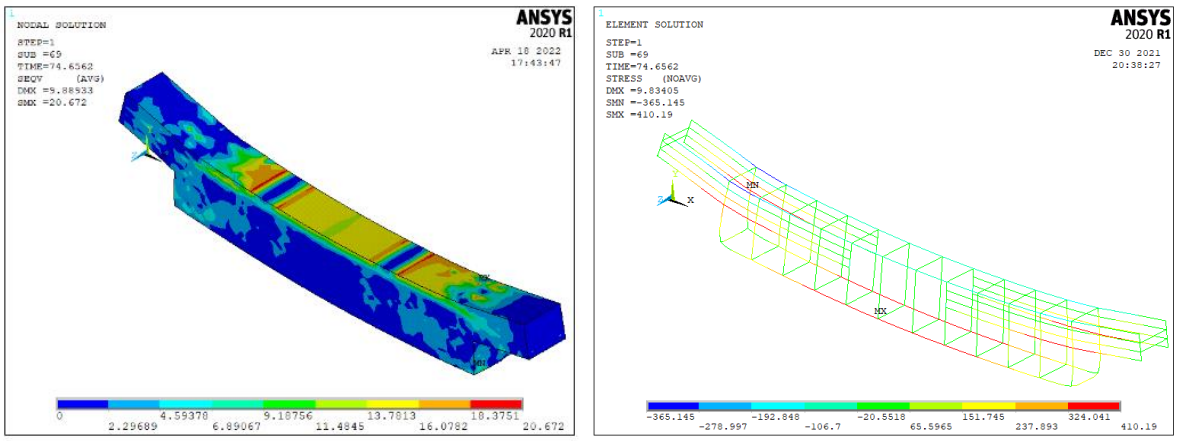

(a) (b)

Figure 13. Stresses in FE model group IV. (a) Concrete Von Mises stresses, (b) Steel stresses

From **Fig. 10-a**, it can be observed that the maximum stress in the concrete of group I is equal to 21.81 MPa, which is 87.2% of the compressive strength (f_c') of concrete used in the analysis (25 MPa). **Fig. 12-b** shows that both main and flexure reinforcement yielded at failure load. It can be seen that the main reinforcement (A_s) yields at the point near the reentrant corner, while the flexure reinforcement yields at the center of the DEB where the constant moment region is. These locations are where we expected yielding would occur. By checking the yielding of the rebars at each load step, we found that the flexure reinforcement yielded before the main reinforcement by two load steps.

Fig. 11 illustrates the stresses of group II, where (a) shows that the maximum stress in concrete is equal to 19.06 MPa, which is 76.2% of the maximum compressive strength (f_c'). And (b) represent the yielding stress in rebars at failure load. Because there is not enough development length of main reinforcement, the bottom line of hoops reinforcement (A_h) yielded only, and its yield stress is equal to 416.628 MPa (104.1% of f_y). This happened because we gave a property of strain hardening to steel reinforcement material during modeling. The other rebars in the section did not reach to yield strength of steel (f_y)which equals 400 MPa.

Fig. 12 illustrates the stresses of group III, where (a) shows that the maximum stress in concrete is equal to 20.5 MPa, which is 82% of the maximum compressive strength. And (b) represent the yielding stress in rebars at failure load. The main and flexure reinforcement yielded at the same location that group I yielded but with higher yield stress which is equal to 528.38 MPa (132.1% of f_y) with 416 MPa for group I. But, in this group, three load steps yielded main reinforcement before flexure reinforcement.

The stresses obtained in group IV are shown in **Fig. 13**. It can be found the maximum stress in concrete is equal to 20.67 MPa, which is 82.6% of the maximum compressive strength, and the rebar yielded at the same location of groups I, III, and the yield stress is equal to 410.19 MPa.

We also note that the stirrups reinforcement of the first group only yields stress equal to 282 MPa, while in the other groups, the stress of stirrups did not exceed 280 MPa, which is the yield strength of stirrups steel.

4.3 Failure Modes and Crack Patterns

The cracking patterns in the FE model could be obtained using the concrete crack/crushing plot option in ANSYS. The four groups showed different modes of failure depending on the reinforcement of each one of them. Final cracks are shown in **Fig. 14** to **Fig. 17**.

(a)

(b)

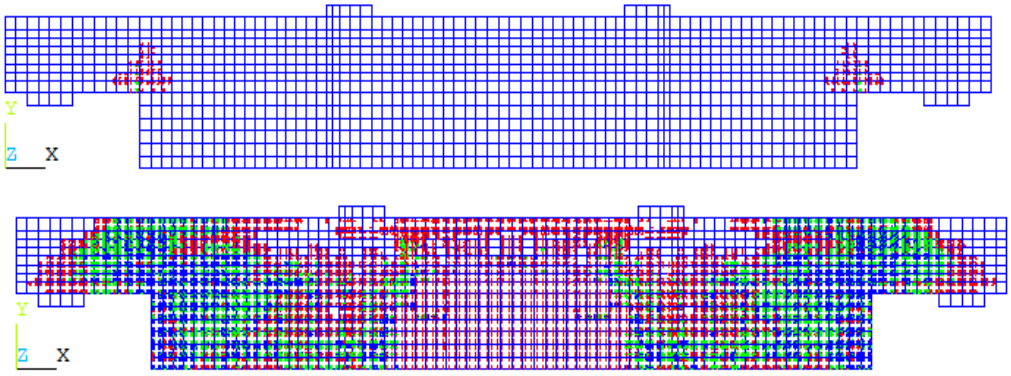

Figure 14. Crack patterns of group I. (a) First Crack, (b) Final Cracks.

(a)

(b)

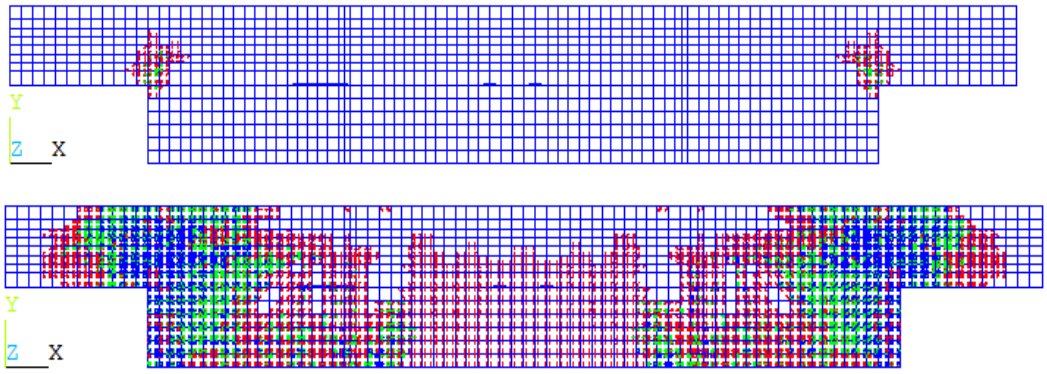

Figure 15. Crack patterns of group II. (a) First Crack, (b) Final Cracks.

(a)

(b)

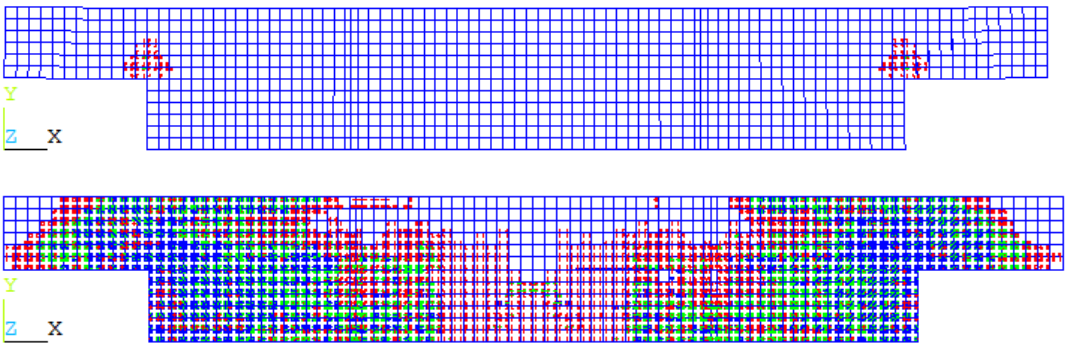

Figure 16. Crack patterns of group III. (a) First Crack, (b) Final Cracks.

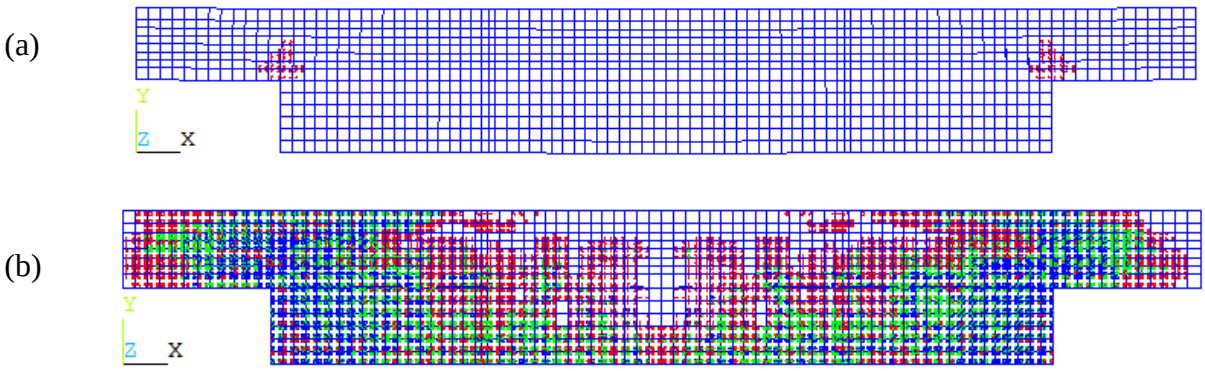

Figure 17. Crack patterns of group IV. (a) First Crack, (b) Final Cracks.

In the nonlinear region of the analysis, consecutively cracks appear as more load is applied to the model. **Fig. 14** through **Fig. 17** shows that numerous cracks occur on the body of DEB.
Fig. 14-a illustrates that the first crack, in group I, starts at the reentrant corner at a load of 16 kN (about 20% of failure load). This crack spreads out at approximately 45° with horizontal and then extends toward the top face of the model. As an applied load is further increased, another type of crack appeared and occurred in the nib portion: diagonal tension and concrete crushing cracks, and the existing cracks lengthen. The diagonal tension crack in the nib assumes a flatter trajectory on reaching the hanger reinforcement, propagating toward the loading plates. This agrees with the strut and tie model (STM) simulation. The final crack happened at 80kN load, as shown in figure 16-b. Approximately all types of cracks are found in this stage of analysis, vertical shear cracks, diagonal tension cracks, concrete crushing cracks, and also flexural cracks that occurred in the midspan of the FE model.
From **Fig. 15**, we can observe another type of cracks which is direct shear cracks found in group II. This happened because the is not enough development length of the main reinforcement beyond the reentrant corner. The final crack in this group occurs at 49.5kN, as shown in figure 15-b.
The first crack in group III is shown in **Fig. 16-a**, which appears at a load of 14.4 kN, about 19% of failure load, and the final crack happened at 76.4 kN as shown in **Fig. 16-b**.
The last group IV, seems to be the same as group III in failure mode, with a difference in the first and final crack stage happening of loading.

5. PARAMETRIC STUDY

As mentioned previously, the control sample is the FE sample of group I that has been verified against the experimental sample, so a parametric study will be conducted on this group to predict the effect of support settlement, high strength concrete, and inclination of applied load on the behavior of the DEB.

5.1 Effect of Support Settlement

Support settlement has a significant effect on the behavior of the structural element under loading. The applied loads are non-uniformly distributed loads on the structure, thus non-uniformly distributed on the foundation and the soil under the structure, without forgetting the non-homogeneity of soil under the structure, which causes differential settlement in the structure and affects the behavior of all structural members including beams with dapped-ends.
In this section, this effect will be studied using the ANSYS program by modeling the elastic supports as springs with a specific stiffness coefficient (K) using the combined14 element, where

the values of the stiffness coefficient (K) are taken to be equal to 100,250,500,1000,2000,3000,4000,5000 and 10,000 N/mm for study.

5.1.1 Load-deflection response

The load-midspan deflection curves for all values of spring constant (K) obtained from finite element analysis are shown in **Fig. 18** and compared with the experimental results in **Table 3.**

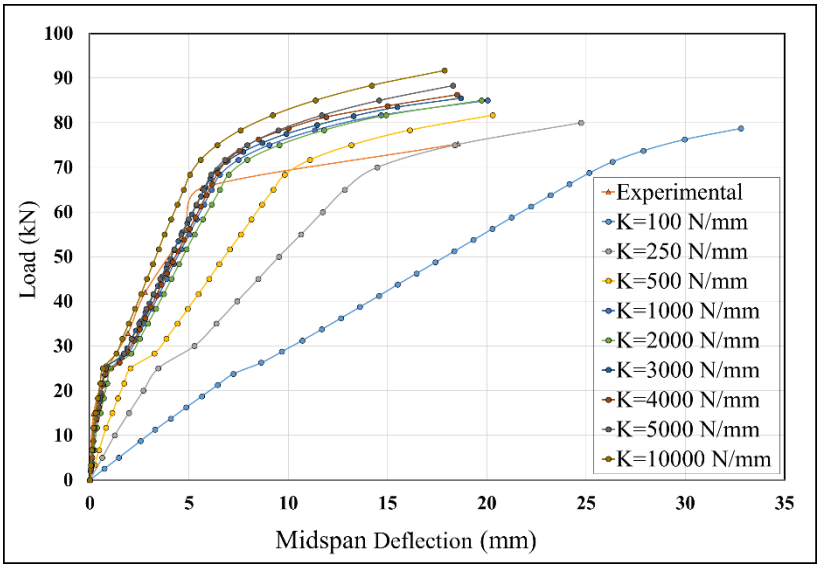

Figure 18. Load-Deflection curves for different spring constant values.

Table 3. Comparison between failure results of experimental and ANSYS models for different spring constant value (K).

K (N/mm)	Experimental Load (kN)	ANSYS Load (kN)	ANSYS / Experimental	Experimental Deflection (mm)	ANSYS Deflection (mm)	ANSYS / Experimental
100	75	78.75	1.05	18.5	32.798	1.77
250	75	80	1.06	18.5	24.746	1.33
500	75	81.667	1.09	18.5	20.292	1.09
1,000	75	85	1.13	18.5	20.04	1.08
2,000	75	85	1.13	18.5	19.742	1.067
3,000	75	85.5	1.14	18.5	18.687	1.01
4,000	75	86.25	1.147	18.5	18.495	0.92
5,000	75	88.333	1.17	18.5	18.287	0.988
10,000	75	91.667	1.22	18.5	17.866	1.016

According to **Fig. 18** and **Table 3**, when K=100 N/mm, it gives a failure load equal to 78.75 kN, which is the minimum value, and midspan deflection equals 32.798 mm, which is the maximum

value but when K increase to 250 N/mm, the failure load increase to 80 kN (1.58% increase) and the deflection decrease to 24.746 mm (25% decrease). It can be concluded that when the spring constant (Stiffness K) increases, the failure load and the obtained deflection decrease, so the stiffness is directly proportional to the force and inversely proportional to the displacement. When stiffness constant was equal to 10,000 N/mm, the analysis gives maximum failure load equals 91.667 kN (16.4% increase) and deflection equals 17.866 mm, which is the minimum value.

5.1.2 Stiffness-settlement curves

Fig. 19 shows the stiffness-settlement curve for different values of spring stiffness (K) between (100 – 10,000) N/mm and the vertical settlement of nodes just above the spring element.

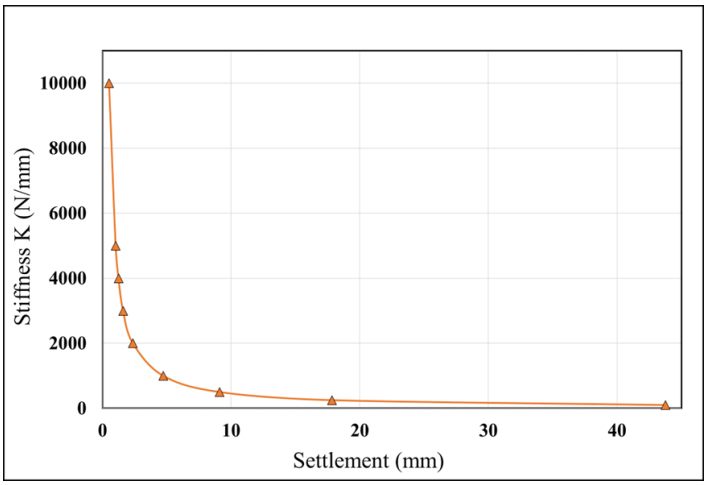

Figure 19. Stiffness-settlement curve for different spring constant values.

Fig. 19 shows that when the spring (K) stiffness increases, the settlement of the node above the spring decreases because their proportionality is inverse. Therefore, when the stiffness was equal to 100 N/mm the settlement was equal to 44 mm, but when the stiffness increased to 10,000 N/mm the settlement dropped to 0.5 mm.

5.2 Effect of Compressive Strength of Concrete (f'_c)

In this section, the effect of changing the value of concrete compressive strength of concrete on the behavior of DEB was studied, and was used concrete with compressive strength (f'_c) equals to 50, 70, and 90 MPa and compare the results with group I, which has concrete compressive strength equal to 25 MPa.

5.2.1 Load-deflection response

The load-deflection curves of the experimental model and the finite element model with concrete compressive strength equal to 25, 50, 70 and 90 MPa are shown in **Fig. 20**.

Table 4 shows the failure loads and deflection and the percentage of increase in failure load and deflection due to an increase in compressive strength for each sample, while **Fig. 21** illustrates the relationship between failure load and compressive strength (f'_c).

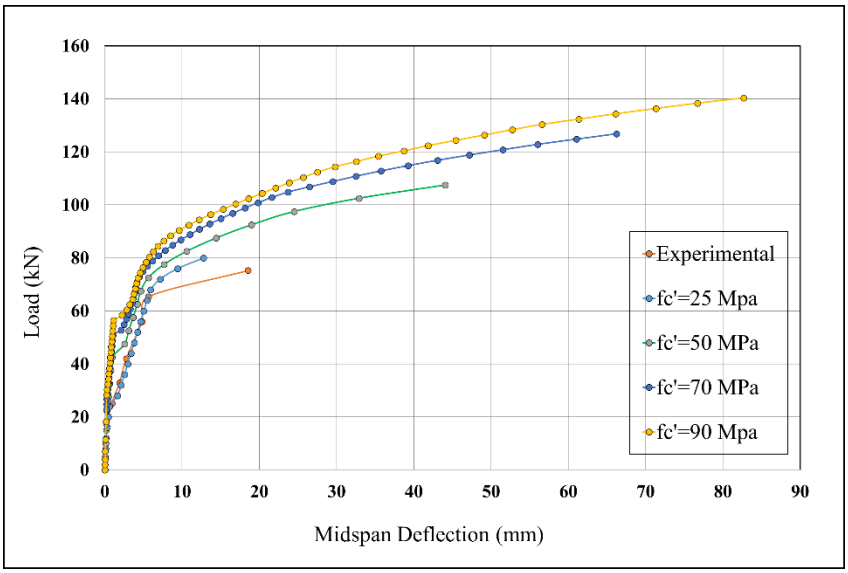

Figure 20. Load-Deflection Curves of high strength concrete.

Table 4. Failure Load deflection and increase in failure load and deflection due to an increase in compressive strength.

f_c' (MPa)	Failure Load (kN)	Max. Deflection (mm)	Percentage of increase in failure load (%)	Percentage of increase in deflection (%)
25	80	12.789	0	0
50	107.5	44.059	34	244
70	110.8	52.67	39	312
90	140.38	82.69	75	547

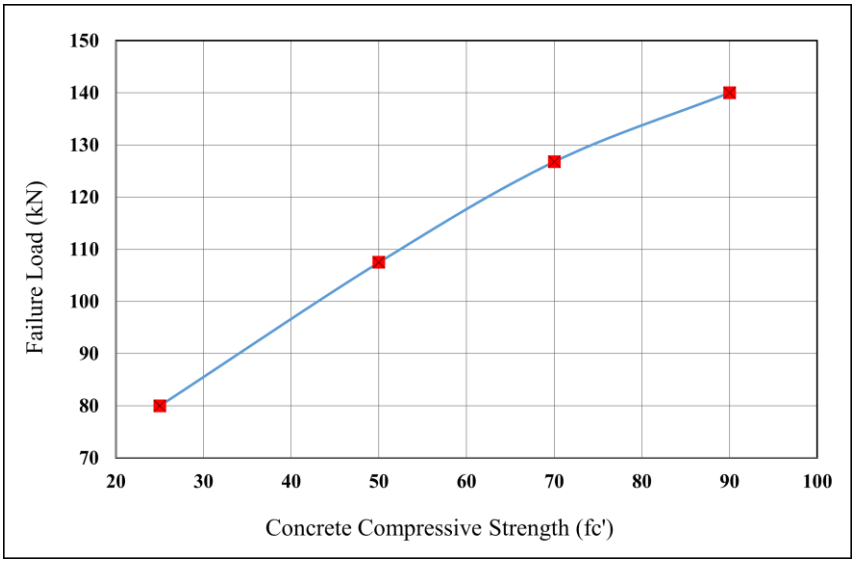

Figure 21. Failure Load-Concrete Compressive Strength Relationship

According to **Fig. 20** and **Fig. 21,** and **Table 4**, the shear strength of DEB increases with the increase of the concrete compressive strength (f_c'). The most obvious increase in strength was

when the compressive strength of concrete was taken to be equal to 90 MPa, that gave increase in failure load by 75% and became equal to 140.38 kN. When the compressive strength was 25 MPa the failure load was equal to 80 kN but when the compressive strength doubled to 50 MPa the failure load increased by 34% and became equal to 107.5 MPa, while when the compressive strength increased to 70 MPa, the failure load increased to 110.8 kN.
As it is obvious from figure 23 and table 6, the midspan deflection increases with increases in concrete compressive strength (f_c').

5.3 Effect of Inclination of Applied Load

In this section, the effect on the behavior of DEB when different angles incline the applied load with horizontal was studied. Such a load may occur in, for example, Gerber's joints or in dapped-end beams supported on corbels. The vertical gravitation force is additionally completed with horizontal forces caused by temperature differences, shrinking, or creeping. The specific angles were 30, 45, 60, and 75 degrees with horizontal.

5.3.1 Load-deflection response

The load-midspan deflection curves for an angle of inclination of the applied load are shown in **Fig. 22**. **Table 5** shows the values of failure load and maximum deflection of each case and compares them with experimental test results.

Table 5. Results of load vertical component and deflection for different load angles.

Results	Experimental	ANSYS 90°	ANSYS 75°	ANSYS 60°	ANSYS 45°	ANSYS 30°
Vertical Component (kN)	75.28	80.00	74.50	64.20	51.70	35.06
Maximum Deflection (mm)	18.55	12.80	11.65	8.80	7.78	4.88

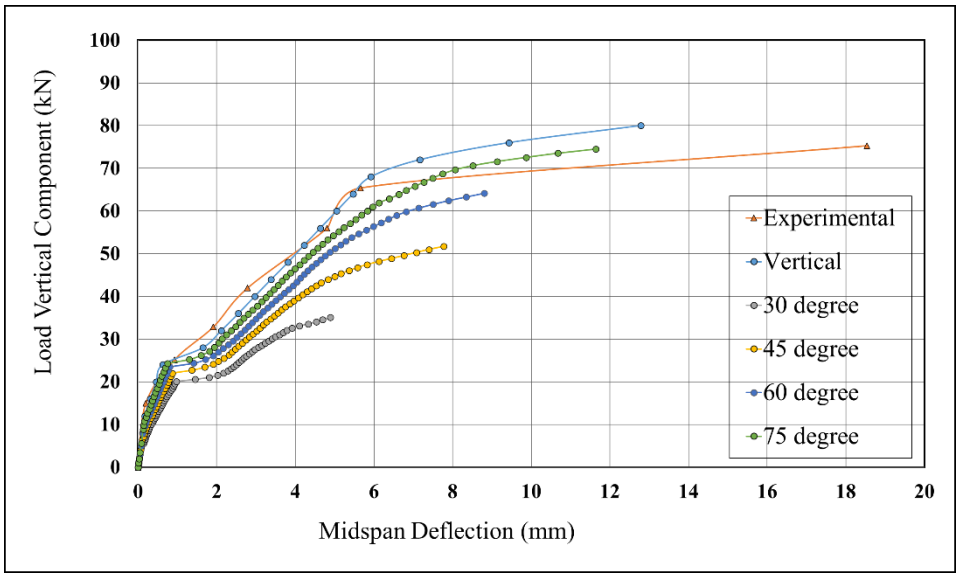

Figure 22. Load vertical component and midspan deflection relationship.

According to **Fig. 22** and **Table 5**, it can be observed that the ultimate failure load decreases with the reduction of the angle of inclination of applied load with the horizontal axis. When the load was vertically applied, the failure load from ANSYS was equal to 80 kN. When it inclined 75° with the horizontal axis (25° with vertical axis), the failure load vertical component was reduced to 74.5 kN (reduction about 6.8%). When the applied load inclined more, 60° with the horizontal axis (30° with the vertical axis), the failure load vertical component reduced more and became equals to 64.2 kN (reduction of about 20%). When the applied load inclined more, 45° with the horizontal axis (45° with the vertical axis), the failure load vertical component reduced more and became equal to 51.7 kN (reduction about 35%). When the applied load was close to horizontal and inclined 30° with the horizontal axis (60° with vertical axis), the failure load vertical component reduced more and became equal to 35.6 kN (reduction of about 55%).
The maximum midspan deflection decreases as the angle of inclination of applied load decrease because at vertical loading, the horizontal component of the load is equal to zero, and this rise the deflection, and as inclination increases, the horizontal component of load increases, and this cause decreasing in deflection.

6. CONCLUSIONS

The following conclusions were drawn from the results of this study:
1. The ANSYS model's load-deflection curves were in good agreement with that of the experimental data. This gave confidence in using ANSYS in representing and analyzing the reinforced concrete dapped-end beams.
2. The failure loads from the finite element model by ANSYS are very close to those of the previous experimental test.
3. The most affected factor on the shear strength of dapped-end beam is the main dapped-end (nib) reinforcement (A_s) and their development length beyond the reentrant corner. The failure load is reduced by 25% when insufficient development length is provided.
4. Nib shear reinforcement has less effect than nib main reinforcement. When the horizontal shear reinforcement at nib (A_h) is eliminated, the failure load was reduced by 4%, while the elimination of vertical shear reinforcement of nib reduced the failure load by 7%.
5. The main dapped-end (nib) reinforcement (A_s) should be positioned as close to the bottom face of the nib as possible, without passing the lower third of the nib depth.
6. The strength of the dapped-ends beams is significantly affected by the differential settlement of the supports. And the shear strength increased by 16%, and deflection decreased by 46% as spring constant (k) increased from 100 to 10,000 N/mm. As the spring constant decreased, the settlement of the node above the spring increased.
7. As concrete compressive strength (f_c') increased, the shear strength of the dapped-ends beam increased. When the compressive strength of concrete increased by 100% led to an enhancement of strength capacity by about 34%, and when the concrete strength increased from 25 MPa to 90 MPa, the failure load increased by 75%.
8- The strength capacity of the dapped-ends beams decreases as the inclination angle of applied load decreases. When the inclination was dropped to 60°, the failure load decreased by 20%, and deflection decreased by 30%.

7. REFERENCES

ACI Committee 318, 2019. Building Code Requirements for Reinforced Concrete (ACI 318M-19), American Concrete Institute, Detroit, Michigan, USA.

AlSabawy A. M., 2013. Nonlinear three-dimensional finite element analysis of reinforced concrete dapped-end beams, *Iraqi journal of civil engineering*, *9*(1), pp.1-16.

Al - Sherrawi, M. H. and Shanshal, Z. M., 2016. Torsional Resistance of Reinforced Concrete Girders with Web Openings, *Journal of Engineering*, 22(2), pp. 137–155.

ANSYS Release Version 15. 2020. A Finite Element Computer Software Theory and User Manual for Nonlinear Structural Analysis. Inc. Canonsburg, PA.

Aswin, M., Mohammed, B.S., Liew, M.S. and Syed, Z.I., 2015. Root cause of reinforced concrete dapped-end beams failure, *International Journal of Applied Engineering Research*, *10*(22), pp.42927-42933.

Chen, W.F., 1982. *Plasticity in reinforced concrete*, J. Ross Publishing.

Desayi, P. and Krishnan, S., 1964, March. Equation for the stress-strain curve of concrete, In *Journal Proceedings*, 61(3), pp. 345-350.

Fib-Bulletin 42, 2008. Constitutive modelling of high strength/ high performance concrete, Fib-International Federation for Structural Concrete Lausanne, Switzerland.

Gere, J. M., and Timoshenko, S. P., 1997. Mechanics of Materials. PWS Publishing Company, Boston, Massachusetts.

Lu, W.Y., Chen, T.C., and Lin, I.J., 2015. Shear strength of reinforced concrete dapped-end beams with shear span-to-depth ratios larger than unity, *Journal of Marine Science and Technology*, *23*(4), pp. 431-442.

Lu, W.Y., Lin, I.J., Hwang, S.J., and Lin, Y.H., 2003. Shear strength of high-strength concrete dapped-end beams, *Journal of the Chinese Institute of Engineers*, *26*(5), pp.671-680.

Mahmood, B.A., and Mohammad, K.I., 2019. Finite element analysis for RC deep beams under an eccentric load, *Tikrit Journal of Engineering Sciences*, *26*(1), pp.41-50.

Mohammed, S. D., and Mahmoud, T. K., 2015. Strength Enhancement of Prestressed Concrete Dapped-End Girders, *Journal of Engineering*, 21(10), pp. 1–16.

Meyer, J., 1998. *Ein Beitrag zur Untersuchung der Verformungsfähigkeit von Bauteilen aus Beton unter Biegedruckbeanspruchung, University of Leipzig* (Doctoral dissertation, PhD thesis.

Nagrodzka-Godycka, Krystyna, and Paweł Piotrkowski, 2012. Experimental Study of Dapped-End Beams Subjected to Inclined Load, *ACI Structural Journal,* 109(1), pp. 11-20.

Pei-Chang Huang and Antonio Nanni, 2015. Dapped-End Strengthening of Precast Prestressed Concrete Double Tee Beams with FRP Composites, Center for Infrastructure Engineering Studies.

Peng T., 2009. Influence of Detailing on Response of Dapped End Beams. A Thesis of Master Degree, Mcgill University, Montréal, Canada. pp. 1-103.

Popovics, S., 1973. A numerical approach to the complete stress-strain curve of concrete, *Cement and concrete research*, *3*(5), pp.583-599.

Precast/Prestressed Concrete Institute, 2010. PCI Design Handbook – Precast and Prestressed Concrete, Seventh Edition, Precast/Prestressed Concrete Institute, Chicago, Illinois, USA.

Sabre, Ahmed Bashar M., Bayar J. Al-Sulayfani, and Khalaf I. Mohammad, 2021. Numerical Study on Nonlinear Behavior of RC Continuous Deep Beams, *Journal of Physics*, 1973(1), pp. 1-17.

Shakir, Q.M., Al-Tameemi, H.A., and Kamonna, H.H., 2020. Effect of Opening Characteristics on the Performance of High Strength Rc Dapped-End Beams, *Journal of Engineering Science and Technology*, *15*(3), pp.693-708.

Shakir, Qasim M., 2018. Reinforced concrete dapped end beams–state of the art, *International Journal of Applied Science* 1(2), pp. 44-57.

Shakir, Qasim M., 2020. A Review on Structural Behavior, Analysis and Design of RC Dapped End Beams, IOP Conference Series: Materials Science and Engineering, 978(1), pp. 1-16.

Taher, S.D., 2005. Strengthening of critically designed girders with dapped ends. *Proceedings of the Institution of Civil Engineers-Structures and Buildings*, *158*(2), pp.141-152.

Wang Q., Guo Z., and Hoogenboom, P. C.J., 2005. Experimental investigation on the shear capacity of RC dapped end beams and design recommendations, *Structural Engineering and Mechanics*, 21(2), pp. 221-235.

Willam, Kaspar J., and Warnke EP., 1975. Constitutive Model for the Triaxial Behavior of concrete, International Association for Bridge and Structural Engineering. 19, pp. 1-30.